AIAA JOURNAL
Vol. 40, No. 4, April 2002

Nonlinear Inviscid Aerodynamic Effects on Transonic Divergence, Flutter, and Limit-Cycle Oscillations

Jeffrey P. Thomas,* Earl H. Dowell,† and Kenneth C. Hall‡
Duke University, Durham, North Carolina 27708–0300

By the use of a state-of-the-art computational fluid dynamic (CFD) method to model nonlinear steady and unsteady transonic flows in conjunction with a linear structural model, an investigation is made into how nonlinear aerodynamics can effect the divergence, flutter, and limit-cycle oscillation (LCO) characteristics of a transonic airfoil configuration. A single-degree-of-freedom (DOF) model is studied for divergence, and one- and two-DOF models are studied for flutter and LCO. A harmonic balance method in conjunction with the CFD solver is used to determine the aerodynamics for finite amplitude unsteady excitations of a prescribed frequency. A procedure for determining the LCO solution is also presented. For the configuration investigated, nonlinear aerodynamic effects are found to produce a favorable transonic divergence trend and unstable and stable LCO solutions, respectively, for the one- and two-DOF flutter models.

Nomenclature

a	=	nondimensional location of airfoil elastic axis, e/b
b, c	=	semichord and chord, respectively
c_l, c_m	=	coefficients of lift and moment about elastic axis, respectively
e	=	location of airfoil elastic axis, measured positive aft of airfoil midchord
h, α	=	airfoil plunge and pitch degrees of freedom
I_α	=	second moment of inertia of airfoil about elastic axis
j	=	$\sqrt{-1}$
K_h	=	airfoil plunge stiffness
K_α	=	airfoil torsional stiffness about elastic axis
M_∞	=	freestream Mach number
m	=	airfoil sectional mass
N	=	number of degrees of freedom of computational fluid dynamics model
N_H	=	number of harmonics
q_∞	=	freestream dynamic pressure
r_α	=	radius of gyration of airfoil about elastic axis, $r_\alpha^2 = I_\alpha/mb^2$
S_α	=	first moment of inertia of airfoil about elastic axis
T	=	period
t	=	time
U_∞	=	freestream velocity
V	=	reduced velocity, $U_\infty/\omega_\alpha c$
x_α	=	airfoil static unbalance, S_α/mb
α_0	=	airfoil steady (mean) flow angle of attack
μ	=	mass ratio, $m/\pi\rho_\infty b^2$
ρ_∞	=	freestream density
ω, $\bar{\omega}$	=	frequency and reduced frequency based on airfoil chord, $\bar{\omega} = \omega c/U_\infty$
ω_h, ω_α	=	uncoupled natural frequency of plunging and pitching about elastic axis, respectively

Subscript

f	=	linear neutral stability (flutter) condition

Introduction

LIMIT-CYCLE OSCILLATIONS (LCO) in aeroelastic systems appear to be more prevalent in transonic flow than in subsonic flow. Hence, it has been thought that, at least for some configurations, the source of the nonlinearity that leads to LCO is in the aerodynamic flow. Of course, nonlinear structural mechanisms can also lead to LCO whether the flow is transonic or not. There have been wind-tunnel experiments where the test model was designed to exhibit LCO due to a structural nonlinearity, and such test results have been successfully correlated with analysis.[1,2] However, the present understanding of LCO induced by aerodynamic nonlinearities is less complete, and, as yet, no systematic quantitative correlation between theory and experiment has been achieved.

This is perhaps a meaningful measure of the greater difficulty in modeling aerodynamic nonlinearities, both theoretically and experimentally, compared to modeling nonlinearities in a structure.

One of the advantages of studying theoretical models is that each of the several possible physical phenomena that may lead to LCO can be studied separately. In this paper, we consider the effects of nonlinearities arising from inviscid transonic aerodynamics. The principal physical effect of interest is the relatively large motion of the shock wave as the amplitude of the pitch motion of the airfoil, for example, becomes sufficiently large. This in turn leads to a movement of the center of pressure with amplitude. Hence, one expects to see an effect of amplitude on the neutrally stable motions that may occur. Moreover, this may lead to limit-cycle motions rather than the catastrophic exponentially growing oscillations predicted by time linearized aerodynamic models. The latter models capture the effect of the mean position of the shock and small shock motions about this mean position by assuming that the shock motion is dynamically linear, that is, the shock motion is proportional to the airfoil motion. This is not true for dynamically nonlinear aerodynamic models that allow for larger and more general shock motions, including the possible appearance and disappearance of a shock during a cycle of airfoil motion. The latter is our concern here.

Technical Discussion

In this paper, we consider two distinct aeroelastic phenomena, divergence and flutter, and their associated LCO. To keep the discussion focused on the fundamental physical phenomena, and to ease the interpretation of the inherently complex phenomena, only a single structural degree of freedom will be studied for the divergence case. However, one- and two-degree-of-freedom systems are presented for the case of flutter. The aerodynamic model is a

Received 10 May 2001; revision received 3 October 2001; accepted for publication 3 October 2001.

*Research Assistant Professor, Department of Mechanical Engineering and Materials Science. Member AIAA.

†J. A. Jones Professor, Department of Mechanical Engineering and Materials Science and Dean Emeritus, School of Engineering. Fellow AIAA.

‡Professor, Department of Mechanical Engineering and Materials Science. Associate Fellow AIAA.

state-of-the-art computational fluid dynamics (CFD) method based on the Euler equations of nonlinear, rotational inviscid aerodynamic theory.

Here we emphasize that the solution technique is for a large system of ordinary differential equations in time, which represents the time variation of the fluid unknowns at each spatial grid point in the CFD model. The unknowns are four in number at each grid point for a two-dimensional Euler flow, including density, the two scalar components of momentum, and the total energy at each grid point. The present CFD model has about 17,000 total flow variable unknowns, and, therefore, an efficient solution method is imperative to carry out the studies reported here. Furthermore, we acknowledge the limitations of the inviscid approximation in modeling realistic physical flows. Shock-induced boundary-layer separation, for instance, which requires the implementation of a viscous flow model, may have a significant effect on unsteady aerodynamic loading. Research efforts are currently underway to address this issue.

Harmonic Balance Solution in the Frequency Domain

The pioneering work of Ueda and Dowell[3] and Greco et al.[4] should be recalled. Ueda and Dowell[3] used a describing function technique whereby the dominant harmonic was extracted from a time marching CFD model, LTRAN2, using both indicial and harmonic motions of the airfoil. They considered a two-degree-of-freedom typical airfoil section. Greco et al.[4] used the method of harmonic balance to study the unsteady transonic aerodynamics for flutter and LCO prediction. In their work, they used the transonic small disturbance potential flow model, as did Ueda and Dowell,[3] and only considered a single harmonic. In the present work, we employ the Euler equations of fluid dynamics and also retain multiple harmonics in the aerodynamic model. It is found that using several harmonics improves the theoretical prediction of the aerodynamic forces. However, in the aeroelastic analysis, when the fluid and structural models are coupled, only a single harmonic is used for the structural model. Earlier studies of structural nonlinearities support this approximation.[2] The effects of higher harmonics in the aerodynamic model on this single harmonic in the structural model are retained because they are found to be significant in the fluid model.

Aeroelastic System and Its Solution

The structural motion is represented by a one- or two-degree-of-freedom model in pitch and/or plunge (see Fig. 1 for a depiction of the airfoil and the CFD grid used in the numerical calculations). By carefully selecting the pitch axis and mass ratio, we can ensure that the system will undergo either classical linear aeroelastic divergence or flutter. Divergence can occur when the aerodynamic negative stiffness overcomes the structural stiffness, and flutter may occur when the aerodynamic negative damping overcomes the structural damping. As will be shown, each of these classical linear aeroelastic phenomena has a distinctively different limit-cycle or nonlinear behavior.

The Mach number for these studies is $M_\infty = 0.8$ and a NACA 64A010A airfoil is considered. The NACA 64A010A is a symmetric (10.6% thickness ratio) variant of the "Ames" AGARD 156 (see Ref. 5) benchmark section. An O-type computational mesh with 65×65 radial and circumferential nodes that has an outer boundary radius of 10 chord lengths is used for the CFD calculations. The computed static pressure distribution for an angle of attack of 0.0 and 5.0 deg is shown in Fig. 2. Note that at 5.0 deg, the upper surface shock wave has moved rearward and increased in strength, and, on the lower surface, the shock has essentially disappeared. The center of pressure $x_{c.p.}$ as a function of static angle of attack is shown Fig. 3, where it is seen that the center of pressure moves from 32% chord to 40% chord as the angle of attack varies from 0.0 to 5.0 deg.

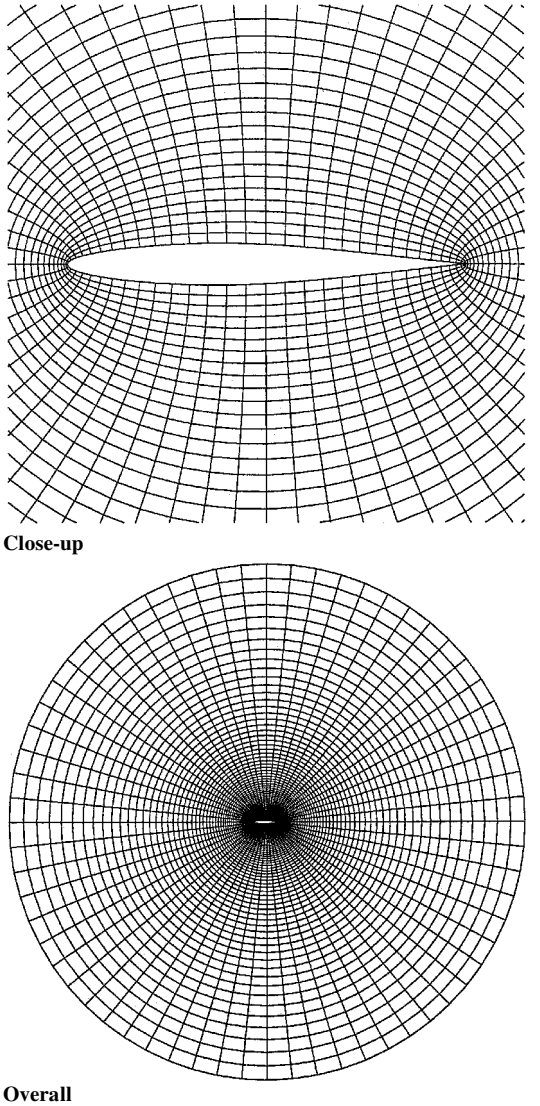

Fig. 1 NACA 64A010A computational grid.

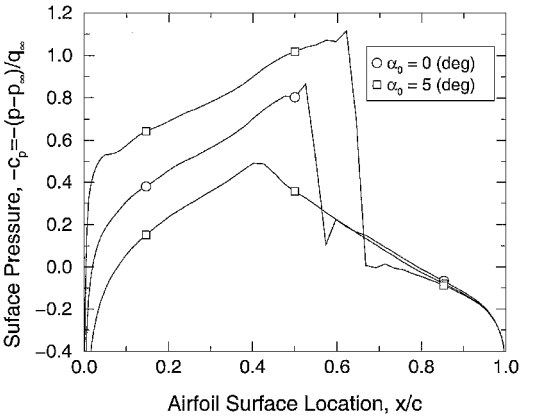

Fig. 2 Steady flow surface pressure distributions: NACA 64A010A airfoil section, $M_\infty = 0.8$.

Linear and Nonlinear Divergence

This is perhaps the simpler of the two phenomena because, by definition, it is time independent, that is, we are dealing with a static linear instability and its nonlinear counterpart. In this case, the single structural equation of motion in pitch about the midchord becomes an equation of static equilibrium. For the aerodynamic model, we only need to determine the lift and moment about some appropriate axis as a function of angle of attack. For small angle of attack, we will recover the classical linear aeroelastic divergence phenomena. However, the question is, what are the effects of the nonlinearity?

The equation of static equilibrium simply equates the aerodynamic and elastic restoring moments. Namely,

$$K_\alpha \alpha = q_\infty c^2 c_m(\alpha) \tag{1}$$

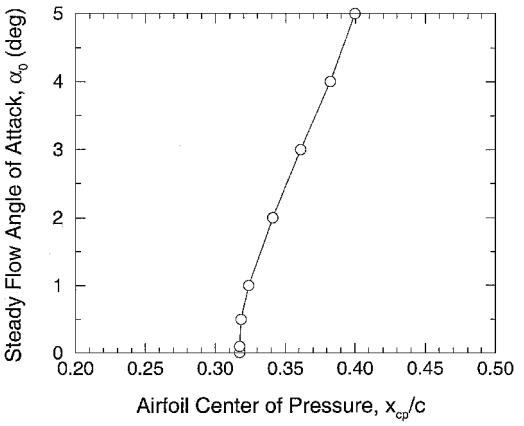

Fig. 3 Center of pressure variation with angle of attack: NACA 64A010A airfoil section, $M_\infty = 0.8$.

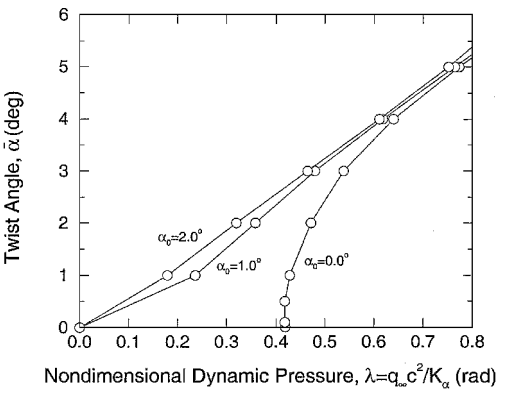

Fig. 4 Divergence and postdivergence of an airfoil, including transonic nonlinear inviscid aerodynamics: NACA 64A010A airfoil section, $M_\infty = 0.8$ and $a = 0.0$.

When a nondimensional dynamic pressure λ is defined, Eq. (1) may be rewritten as

$$\lambda = \alpha / c_m(\alpha) \tag{2}$$

where λ is given by $\lambda = q_\infty c^2/K_\alpha$. The angle of attack may have an initial angle α_0, which is prescribed, and also an additional angle due to the torsional twist of the elastic spring α.

Now, for a linear aeroelastic model, the aerodynamic moment coefficient is simply proportional to the angle of attack. Thus, for no initial angle of attack, the classical linear divergence dynamic pressure is given by Eq. (2), where λ is now a fixed number.

To extend this study of divergence into the nonlinear range, we recognize that now the aerodynamic coefficient is a nonlinear function of angle of attack. For zero initial angle of attack, we may determine the twist of the torsional spring, and its dependence on λ, by specifying the twist angle in Eq. (2) and then solving for λ. This procedure is readily extended to the case with an initial angle of attack.

Qualitatively one can anticipate the effect of the aerodynamic nonlinearity by examining the aerodynamic moment variation with angle of attack. A necessary condition for divergence to occur is that the aerodynamic moment be positive in the same direction as the twist angle. Moreover, if the nonlinear aerodynamic model predicts a moment less in magnitude than that predicted by linear aerodynamic theory, the effect of the nonlinearity will be to stabilize the divergence and vice versa if the nonlinear theory predicts an increase in aerodynamic moment over that given by linear theory. Hence, by examining the slope of the moment vs angle-of-attack curve with increasing angle of attack, we will know whether the effect of the nonlinearity is favorable or unfavorable.

In the following example, the effect is favorable. That is, once the divergence dynamic pressure for a small angle of attack is exceeded (this is the classical linear aeroelastic divergence dynamic pressure), then the angle of twist of the pitch spring remains finite and smoothly increases from zero beyond the divergence dynamic pressure (see Fig. 4, where the angle of twist is plotted vs the nondimensional dynamic pressure). Also shown are results with an initial angle of attack. In this latter case, there is some twist over the full range of dynamic pressure. Indeed, even if the initial angle of attack is only a few degrees, it would be difficult to detect the classical divergence dynamic pressure experimentally for this example. For readers who have studied buckling of systems in the presence of imperfections (e.g. beams, plates, or shells with initial curvature), this behavior will be familiar.

In this example, recall that the center of pressure moves from 32% chord at low angles of attack to 40% chord at 5.0-deg angle of attack. This is the principal reason for the stabilizing effect of nonlinear aerodynamics on the postdivergence condition.

Had the change of the slope of the aerodynamic moment curve been in the opposite direction, then the angle of twist vs dynamic pressure curve would have bent the other way. That is, for dynamic pressures below the classical divergence dynamic pressure, there would be nontrivial (nonzero) twist angles that represent possible static nonlinear equilibrium solutions. Intuitively, one recognizes that these latter solutions would themselves be unstable, that is, such results would be interpreted physically as the magnitude of the disturbance required to generate nontrivial twist at dynamic pressures below the classical divergence dynamic pressure. In our studies to date, only the stable nonlinear effect has been observed for statically divergent systems. However, this is not to say that unstable nonlinear divergence systems may not be encountered for some other parameter combinations.

Of course, divergence is a very special case of nonlinear aeroelasticity as it is for linear aeroelasticity because the frequency of oscillation is zero when divergence and postdivergence occurs. Thus, we now turn to an oscillatory case. First we consider the nonlinear unsteady aerodynamic model and its solution via a harmonic balance method.

Harmonic Balance Methodology

First consider the development of the harmonic balance formulation for the case of three-dimensional flows with moving boundaries. For generality, we present the development in three dimensions, which can be written in a more compact form than for two-dimensions. This methodology has been recently devised by Hall et al.[6] and has been used to model nonlinear unsteady periodic flows in cascade compressors. McMullen et al.[7] have also recently investigated using a variation technique as a method to accelerate convergence to a periodic steady state in turbomachinery flows.

Governing Equations

We consider the inviscid Euler equations (the Navier–Stokes equations can be treated in a similar manner), which may be written in integral form as

$$\frac{\partial}{\partial t}\int\int\int_{V(t)} \boldsymbol{U}\,\mathrm{d}V + \int\int_{A(t)} (\vec{\boldsymbol{\mathcal{F}}} - \boldsymbol{U}\vec{\boldsymbol{x}})\cdot\hat{\boldsymbol{n}}\,\mathrm{d}A = \boldsymbol{0} \tag{3}$$

where $\boldsymbol{U}$ is the vector of conservative fluid variables

$$\boldsymbol{U} = \{\rho \quad \rho u \quad \rho v \quad \rho w \quad E_t\}^T \tag{4}$$

$$\vec{\boldsymbol{\mathcal{F}}} = \boldsymbol{F}\hat{i} + \boldsymbol{G}\hat{j} + \boldsymbol{H}\hat{k} \tag{5}$$

where $\boldsymbol{F}$, $\boldsymbol{G}$, and $\boldsymbol{H}$ are the x, y, and z direction component flux vectors, that is,

$$\boldsymbol{F} = \begin{Bmatrix} \rho u \\ \rho u^2 + p \\ \rho uv \\ \rho uw \\ (E_t + p)u \end{Bmatrix}, \qquad \boldsymbol{G} = \begin{Bmatrix} \rho v \\ \rho uv \\ \rho v^2 + p \\ \rho vw \\ (E_t + p)v \end{Bmatrix}$$

$$\boldsymbol{H} = \begin{Bmatrix} \rho w \\ \rho uw \\ \rho uv \\ \rho v^2 + p \\ (E_t + p)w \end{Bmatrix}$$

The unsteady motion of the control volume $\vec{x}$ is given by

$$\vec{x} = f\hat{i} + g\hat{j} + h\hat{k} \tag{6}$$

and this accounts for the effect of airfoil motion.

Fourier Series Expansion

We consider the unsteadiness of the flow to be strictly periodic in time with period $T = 2\pi/\omega$, where ω is the fundamental unsteady frequency. As such, we may expand Eq. (3) in a Fourier series. For instance,

$$\iiint_{V(t)} \boldsymbol{U}\,\mathrm{d}V = \boldsymbol{Q}(t) \approx \sum_{n=-N_H}^{N_H} \hat{\boldsymbol{Q}}_n e^{jn\omega t} \tag{7}$$

so that

$$\frac{\partial}{\partial t}\iiint_{V(t)} \boldsymbol{U}\,\mathrm{d}V \approx j\omega \sum_{n=-N_H}^{N_H} n\hat{\boldsymbol{Q}}_n e^{jn\omega t} \tag{8}$$

and, similarly,

$$\iint_{A(t)} (\vec{\mathcal{F}} - \boldsymbol{U}\vec{x})\cdot\hat{\boldsymbol{n}}\,\mathrm{d}A = \boldsymbol{R}(t) \approx \sum_{n=-N_H}^{N_H} \hat{\boldsymbol{R}}_n e^{jn\omega t} \tag{9}$$

N_H is the number of harmonics used in the Fourier expansion.

Fourier Coefficients

Substituting the Fourier expansions [Eqs. (8) and (9)] into Eq. (3), multiplying by $e^{-jm\omega t}$, and integrating over one period, that is,

$$\int_0^T \frac{1}{T}\sum_{n=-N_H}^{N_H} (jn\hat{\boldsymbol{Q}}_n + \hat{\boldsymbol{R}}_n)e^{jn\omega t}e^{-jm\omega t}\,\mathrm{d}t \tag{10}$$

yields a system of equations for the Fourier coefficients. Namely,

$$\boldsymbol{A}\hat{\boldsymbol{Q}} + \hat{\boldsymbol{R}} = \boldsymbol{0} \tag{11}$$

where

$$\boldsymbol{A} = \begin{bmatrix} -jN_H & & \\ & \ddots & \\ & & jN_H \end{bmatrix}$$

$$\hat{\boldsymbol{Q}} = \begin{Bmatrix} \hat{\boldsymbol{Q}}_{-N_H} \\ \hat{\boldsymbol{Q}}_{-N_H+1} \\ \vdots \\ \hat{\boldsymbol{Q}}_{N_H} \end{Bmatrix}, \qquad \hat{\boldsymbol{R}} = \begin{Bmatrix} \hat{\boldsymbol{R}}_{-N_H} \\ \hat{\boldsymbol{R}}_{-N_H+1} \\ \vdots \\ \hat{\boldsymbol{R}}_{N_H} \end{Bmatrix}$$

Time-Domain Variables

Via a Fourier transform matrix $\boldsymbol{E}$, one can relate the Fourier coefficient variables to solution variables at discrete subtime levels within a given period of motion, that is,

$$\hat{\boldsymbol{Q}} = \boldsymbol{E}\tilde{\boldsymbol{Q}}, \qquad \hat{\boldsymbol{R}} = \boldsymbol{E}\tilde{\boldsymbol{R}} \tag{12}$$

where

$$\tilde{\boldsymbol{Q}} = \begin{Bmatrix} \boldsymbol{Q}(t_0) \\ \boldsymbol{Q}(t_1) \\ \vdots \\ \boldsymbol{Q}(t_{2N_H}) \end{Bmatrix}, \qquad \tilde{\boldsymbol{R}} = \begin{Bmatrix} \boldsymbol{R}(t_0) \\ \boldsymbol{R}(t_1) \\ \vdots \\ \boldsymbol{R}(t_{2N_H}) \end{Bmatrix} \tag{13}$$

$$t_n = \frac{2\pi n}{(2N_H+1)\omega}, \qquad n = 0, 1, \ldots, 2N_H \tag{14}$$

More specifically,

$$\tilde{\boldsymbol{Q}} = \begin{Bmatrix} \iiint_{V(t_0)} \boldsymbol{U}(t_0)\,\mathrm{d}V \\ \iiint_{V(t_1)} \boldsymbol{U}(t_1)\,\mathrm{d}V \\ \vdots \\ \iiint_{V(t_{2N_H})} \boldsymbol{U}(t_{2N_H})\,\mathrm{d}V \end{Bmatrix} \tag{15}$$

$$\tilde{\boldsymbol{R}} = \begin{Bmatrix} \iint_{A(t_0)} [\vec{\mathcal{F}}(t_0) - \boldsymbol{U}(t_0)\vec{x}(t_0)]\cdot\hat{\boldsymbol{n}}(t_0)\,\mathrm{d}A \\ \iint_{A(t_1)} [\vec{\mathcal{F}}(t_1) - \boldsymbol{U}(t_1)\vec{x}(t_1)]\cdot\hat{\boldsymbol{n}}(t_1)\,\mathrm{d}A \\ \vdots \\ \iint_{A(t_{2N_H})} [\vec{\mathcal{F}}(t_{2N_H}) - \boldsymbol{U}(t_{2N_H})\vec{x}(t_{2N_H})]\cdot\hat{\boldsymbol{n}}(t_{2N_H})\,\mathrm{d}A \end{Bmatrix} \tag{16}$$

Thus,

$$\boldsymbol{AE}\tilde{\boldsymbol{Q}} + \boldsymbol{E}\tilde{\boldsymbol{R}} = \boldsymbol{0} \tag{17}$$

$$\boldsymbol{E}^{-1}\boldsymbol{AE}\tilde{\boldsymbol{Q}} + \boldsymbol{E}^{-1}\boldsymbol{E}\tilde{\boldsymbol{R}} = \boldsymbol{0} \tag{18}$$

Now one can work in terms of the time domain variables, which is, in general, much easier to do. The resulting system of equations can be written as

$$\boldsymbol{D}\tilde{\boldsymbol{Q}} + \tilde{\boldsymbol{R}} = \boldsymbol{0} \tag{19}$$

where

$$\boldsymbol{D} = \boldsymbol{E}^{-1}\boldsymbol{AE} \tag{20}$$

Pseudotime Marching

By adding a pseudotime derivative term $\delta\tilde{\boldsymbol{Q}}/\delta t$ to Eq. (19), one can develop an iterative technique for determining the solution $\tilde{\boldsymbol{Q}}$. Namely,

$$\frac{\delta\tilde{\boldsymbol{Q}}}{\delta t} + \boldsymbol{D}\tilde{\boldsymbol{Q}} + \tilde{\boldsymbol{R}} = \boldsymbol{0} \tag{21}$$

Thus, for example, in the case of a finite volume based CFD method, Eq. (21) would be solved for every computational finite volume comprising the computational mesh. The overall method would, thus, consist of pseudotime marching $N \times (2N_H + 1)$ dependent variables, where N is the number of mesh points times the number of dependent variables. Note that modifying an existing CFD flow solver to implement the harmonic balance technique is a relatively straightforward task because the main requirement is just a redimensioning of the primary arrays from N elements to $N \times (2N_H + 1)$ elements. The rest of the flow solver can remain relatively unchanged because the unsteadiness is due primarily to the source term $\boldsymbol{D}\tilde{\boldsymbol{Q}}$.

Flutter and Associated LCO

Now consider single-degree-of-freedom flutter in pitch. Here, the classical flutter arises from a negative damping in the aerodynamic moment beyond a certain reduced frequency. However, the reduced frequency at which the aerodynamic damping moment becomes negative increases as the angle of pitch oscillation increases. Hence, the reduced velocity decreases as the angle of pitch increases, which suggests that this will lead to an unstable LCO, as indeed it does.

In the example considered, we have moved the elastic axis to 20% chord to preclude divergence and to induce flutter.

Note that in the present analysis, we are using a single harmonic to represent the pitch oscillation. However, in the calculation of the aerodynamic moment, we have included up to three harmonics to determine the effect of higher harmonics on the first harmonic of the aerodynamic moment. It turns out that the effect of the third harmonic is negligible. Indeed, if one only retains a single harmonic in the aerodynamic analysis, the results are qualitatively correct and have fair quantitative accuracy.

Results for the first harmonic for the lift and moment about the pitch or elastic axis are shown in Fig. 5. These results are for two harmonics retained in the aerodynamic analysis. Note that the results at a reduced frequency of zero were those used in the divergence analysis discussed earlier. Of course, a transformation of the pitch axis is used for the divergence analysis.

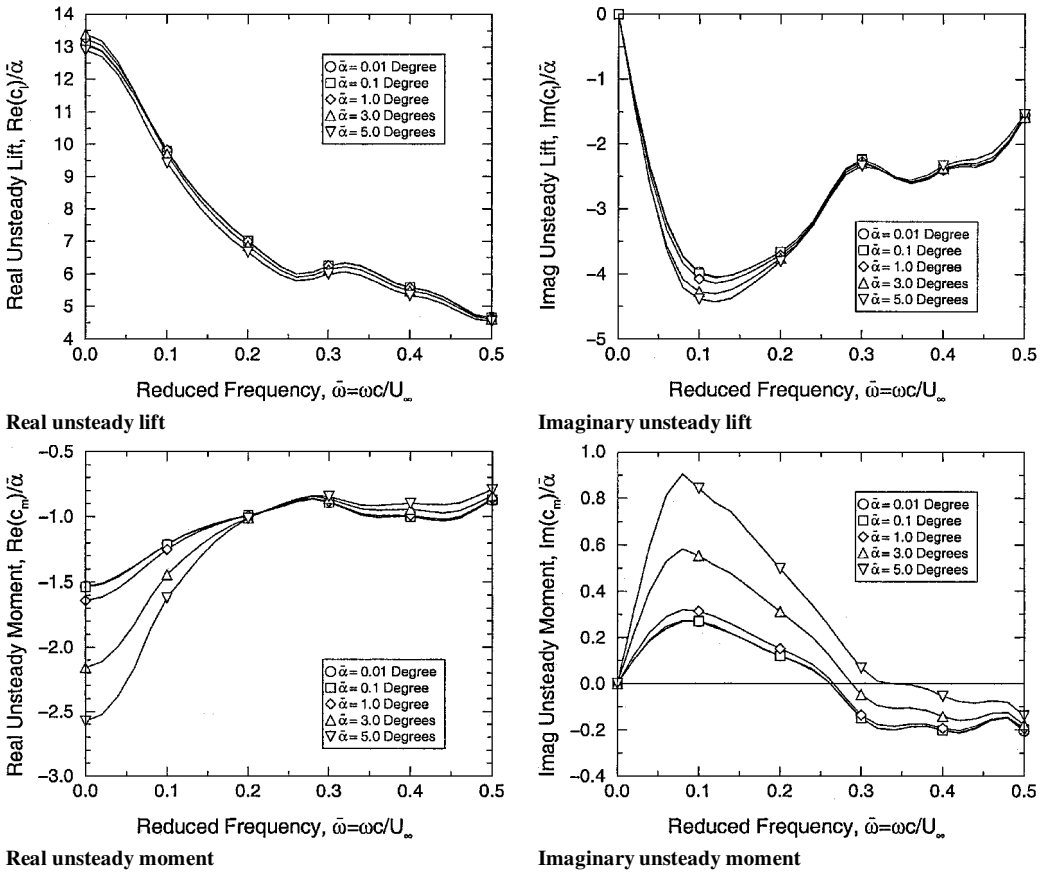

Fig. 5 Unsteady lift and moment for various pitch amplitudes: NACA 64A010A airfoil section, $M_\infty = 0.8$, $\alpha_0 = 0.0$ deg, and $a = -0.6$; two harmonics employed in harmonic balance expansion.

With the real and imaginary parts of the aerodynamic moment taken from Fig. 5, and using the usual pitch equation of motion,

$$I_\alpha\left(\ddot{\alpha} + 2\zeta_\alpha\omega_\alpha\dot{\alpha} + \omega_\alpha^2\alpha\right) = q_\infty c^2 c_m \tag{22}$$

where $\omega_\alpha^2 = K_\alpha/I_\alpha$, we can convert this equation into the frequency domain, nondimensionalize, and separate it into real and imaginary parts. With some rearrangement, these two equations can be written as

$$\left(\frac{\omega_\alpha}{\omega}\right)^2 = 1 + \left(\frac{8}{\pi}\right)\left(\frac{1}{\mu r_\alpha^2}\right)\left\{\frac{\mathrm{Re}[\bar{c}_m(\bar{\alpha},\bar{\omega})]}{\bar{\alpha}\bar{\omega}^2}\right\} \tag{23}$$

$$\zeta_\alpha = \left(\frac{8}{\pi}\right)\left(\frac{1}{\mu r_\alpha^2}\right)\left(\frac{V}{\bar{\omega}}\right)\left\{\frac{\mathrm{Im}[\bar{c}_m(\bar{\alpha},\bar{\omega})]}{\bar{\alpha}}\right\} \tag{24}$$

where a bar over the aerodynamic coefficient and angle of twist denotes the amplitude of the first harmonic and Re and Im denote real and imaginary parts.

The imaginary part of the equation of motion [Eq. (24)] essentially determines the neutral stability condition of the system, and the real part determines the frequency of oscillation. Of course, now both of these results depend on the pitch amplitude $\bar{\alpha}$ of motion.

Although structural damping is readily included in the analysis, as will be seen hereafter, it will be helpful to understand the essence of the results by first considering the solution for zero structural damping.

Zero Structural Damping

In this case, Eq. (24) states that a neutrally stable oscillation will occur when the imaginary part of the aerodynamic moment becomes zero. This will occur at some reduced frequency for a particular angle of pitch oscillation (and other parameters fixed such as Mach number). Then, from Eq. (23), one can solve for the frequency of this neutrally stable oscillation. For sufficiently small motions, this is the flutter solution; for larger motions, we determine an LCO. The solution procedure then is to select an amplitude of oscillation, determine the reduced frequency at which the imaginary part of the aerodynamic moment is zero from Fig. 5, and then determine the frequency of the oscillation from Eq. (23). Note that this is essentially the same computational procedure as for a classical flutter solution, except that now the reduced frequency, the frequency of oscillation, and the reduced velocity are all functions of the pitch amplitude.

Note, however, that just because the imaginary part of the aerodynamic moment vanishes (i.e., the aerodynamic damping becomes zero), that alone does not ensure that a neutrally stable oscillation will occur. This is because the frequency determined from Eq. (23) must be physically possible, that is, the right-hand side of Eq. (23) must be positive. It is evident that the right-hand side of Eq. (23) depends only on the reduced frequency (which is known by the requirement that the imaginary part of the aerodynamic moment be zero) and a nondimensional moment of inertia. Of course, these reduced frequencies themselves depend on the pitch amplitude. Thus, one can determine when the right-hand side of Eq. (23) is positive or negative and express the result in terms of pitch amplitude and moment of inertia. This relationship is shown in Fig. 6, and the regions where flutter and LCO are or are not possible are indicated. The value of moment of inertia that marks the boundary between no flutter or LCO possible and possible flutter or LCO is termed the asymptotic value.

Large Pitch Moment of Inertia

Now, if the mass ratio or moment of inertia is much larger than the asymptotic value, a not uncommon circumstance, then the flutter or LCO frequency is simply equal to the structural pitch natural frequency [see Eq. (23)]. With this approximation, the results of Fig. 7 are obtained for both zero and nonzero structural damping. Note that the curves bend to the left, which is indicative of an unstable LCO. That is, these results are to be interpreted as the amplitude of a disturbance required to initiate explosive flutter below the classical flutter velocity for this single-degree-of-freedom pitch oscillation.

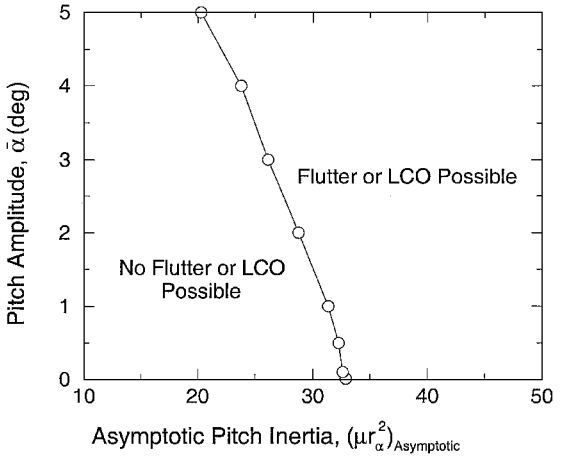

Fig. 6 Asymptotic value of pitch inertia for various pitch amplitudes marking regions where flutter and LCO are or are not possible: NACA 64A010A airfoil section, $M_\infty = 0.8$, $\alpha_0 = 0.0$ deg, and $a = -0.6$.

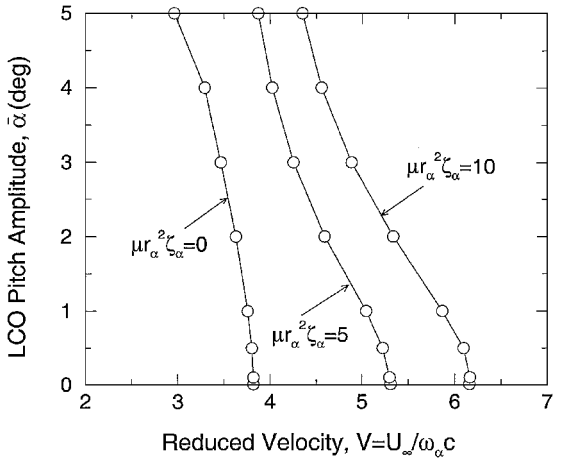

Fig. 7 LCO amplitude vs reduced velocity: NACA 64A010A airfoil section, $M_\infty = 0.8$, $\alpha_0 = 0.0$ deg, and $a = -0.6$.

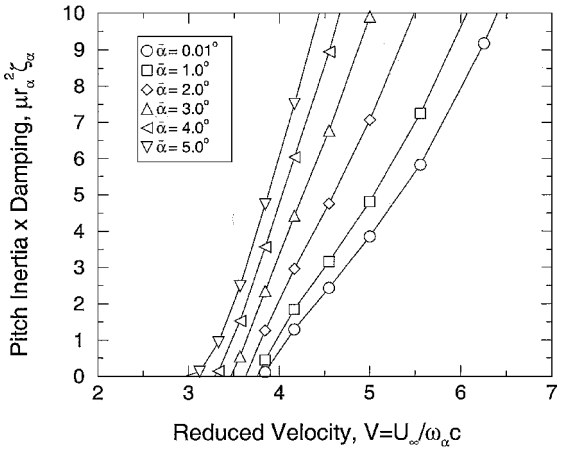

Fig. 8 Normalized structural damping corresponding to neutrally stable LCO for large pitch moment of inertia: NACA 64A010A airfoil section, $M_\infty = 0.8$, $\alpha_0 = 0.0$ deg, and $a = -0.6$.

In Fig. 8, the values of structural damping (normalized by pitch moment of inertia) that correspond to neutrally stable LCO are shown. These can be calculated from Eq. (24) as a function of reduced velocity for various pitch amplitudes. A cross-plot of these data is used to construct the plots for nonzero damping values as shown in Fig. 7.

Effects of Finite Pitch Moment of Inertia

For general values of moment of inertia and structural damping, the solution algorithm using Eqs. (23) and (24), proceeds as follows. First select a Mach number and pitch axis and, for a range of pitch amplitudes, determine the first harmonic of the aerodynamic moment (including higher harmonics of the aerodynamic model and their effect on the fundamental harmonic). Then, for a given pitch amplitude, choose a reduced frequency and determine the flutter or LCO frequency from Eq. (23). This frequency will be proportional to the pitch structural frequency, of course. With the flutter or LCO frequency determined, and the reduced frequency selected, one then knows the flow velocity corresponding to the chosen pitch amplitude. Finally, from Eq. (24), determine the structural damping value necessary to give a neutrally stable flutter or LCO. From this perspective, the flutter condition is simply the neutrally stable motion that may exist at small angles of twist, and the LCO are the neutrally stable oscillations that may exist when the pitch amplitude is finite. Of course, the flutter or LCO may become unstable when it is perturbed (e.g., by perturbations in the amplitude of oscillation), and this is indeed the case in the example treated here.

Up to this point, we have assumed that the pitch moment of inertia is well above its asymptotic value. Hence, the flutter frequency is the same as the structural natural pitch frequency.

Now we consider the more general case and a range of pitch inertias such that the flutter frequency is no longer precisely equal to the structural natural frequency in pitch. Results are shown for nondimensional pitch inertias of 200, 100, 50, 37.5, and 25 in Figs. 9 and 10. Figures 9 and 10 show LCO amplitude as a function of reduced velocity and reduced frequency, respectively. The asymptotic pitch inertia results are also shown for reference.

As expected, for sufficiently large pitch inertia, say greater than 200, the asymptotic results are good approximations. However, for pitch inertias less than 100, the results show a more sensitive dependence on pitch moment of inertia. For sufficiently small pitch moment of inertia, of course, no flutter or LCO is possible.

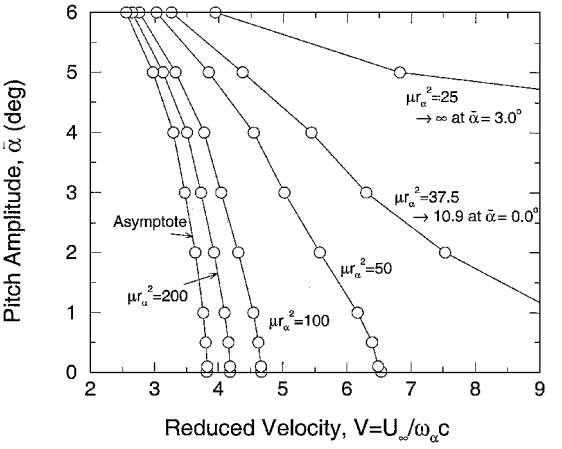

Fig. 9 LCO amplitude vs reduced velocity for various pitch inertias: NACA 64A010A airfoil section, $M_\infty = 0.8$, $\alpha_0 = 0.0$ deg, and $a = -0.6$.

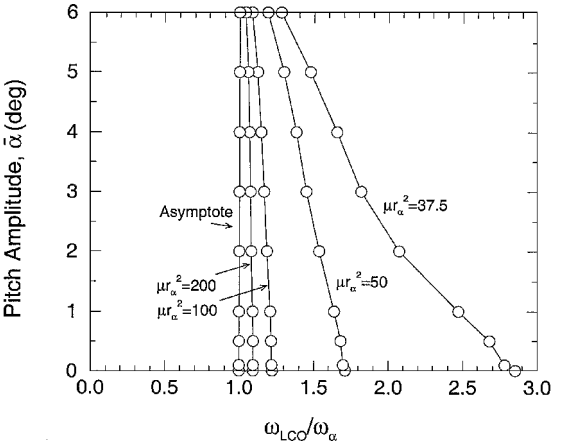

Fig. 10 LCO amplitude vs LCO frequency for various pitch inertias: NACA 64A010A airfoil section, $M_\infty = 0.8$, $\alpha_0 = 0.0$ deg, and $a = -0.6$.

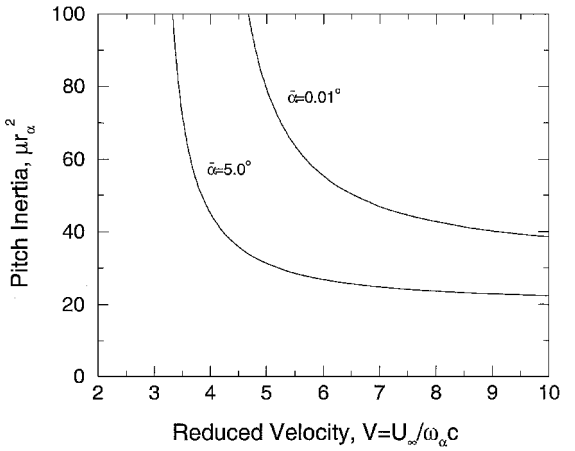

Fig. 11 Pitch inertia vs reduced velocity for fixed pitch amplitudes: NACA 64A010A airfoil section, $M_\infty = 0.8$, $\alpha_0 = 0.0$ deg, and $a = -0.6$.

The relationship between pitch moment of inertia and reduced velocity may be even more clearly seen by fixing the pitch amplitude and then plotting these variables as shown in Fig. 11. Note that in Fig. 11, as reduced velocity decreases, the pitch moment of inertia for flutter and LCO to occur tends to infinity. Thus, for sufficiently small reduced velocity, no flutter or LCO will occur. Conversely, as the pitch moment of inertia decreases, the reduced velocity for flutter or LCO to occur tends to infinity. Thus, below some value of pitch moment of inertia, no flutter or LCO is possible. Of course, these results are for a fixed pitch amplitude when, in fact, the pitch amplitude is an outcome of the analysis (not an input). However, the results are not very sensitive to pitch amplitude, and the conclusions regarding asymptotic behavior hold over the full range of pitch amplitudes considered here.

Multiple Structural Degrees of Freedom

We now consider the case of multiple structural degrees of freedom and examine the two-degree-of-freedom (plunge/pitch) typical airfoil configuration (Fig. 12). The governing equations for this aeroelastic system can be written as

$$m\ddot{h} + S_\alpha \ddot{\alpha} + K_h h = -q_\infty c\, c_l \tag{25}$$

$$S_\alpha \ddot{h} + I_\alpha \ddot{\alpha} + K_\alpha \alpha = q_\infty c^2 c_m \tag{26}$$

As with the single-degree-of-freedom case, we consider harmonically varying excitations, that is, $h = \bar{h}e^{j\omega t}$ and $\alpha = \bar{\alpha}e^{j\omega t}$, and convert the governing equations to the frequency domain. After nondimensionalizing, the system of aeroelastic equations can be written as

$$[-\bar{\omega}^2 \boldsymbol{M} + (1/V^2)\boldsymbol{K}]\boldsymbol{u} = (4/\pi\mu)\boldsymbol{f} \tag{27}$$

where

$$\boldsymbol{M} = \begin{bmatrix} 1 & x_\alpha \\ x_\alpha & r_\alpha^2 \end{bmatrix}, \qquad \boldsymbol{K} = \begin{bmatrix} (\omega_h/\omega_\alpha)^2 & 0 \\ 0 & r_\alpha^2 \end{bmatrix} \tag{28}$$

$$\boldsymbol{u} = \begin{Bmatrix} \bar{h}/b \\ \bar{\alpha} \end{Bmatrix}, \qquad \boldsymbol{f} = \begin{Bmatrix} -\bar{c}_l \\ 2\bar{c}_m \end{Bmatrix} \tag{29}$$

Dynamically Linear Aerodynamics

In the case of a dynamically linear aerodynamic approximation, the right-hand side aerodynamic force vector $\boldsymbol{f}$ can be written as

$$\boldsymbol{f} = \boldsymbol{E}(\bar{\omega})\boldsymbol{u} \tag{30}$$

where $\boldsymbol{E}(\bar{\omega})$ is the 2×2 matrix of aerodynamic transfer functions

$$\boldsymbol{E}(\bar{\omega}) = \begin{bmatrix} -\bar{c}_{l_{\bar{h}/b}}(\bar{\omega}) & -\bar{c}_{l_{\bar{\alpha}}}(\bar{\omega}) \\ 2\bar{c}_{m_{\bar{h}/b}}(\bar{\omega}) & 2\bar{c}_{m_{\bar{\alpha}}}(\bar{\omega}) \end{bmatrix} \tag{31}$$

Equation (27) can then be written as

$$[-\bar{\omega}^2 \boldsymbol{M} + (1/V^2)\boldsymbol{K}]\boldsymbol{u} = (4/\pi\mu)\boldsymbol{E}(\bar{\omega})\boldsymbol{u} \tag{32}$$

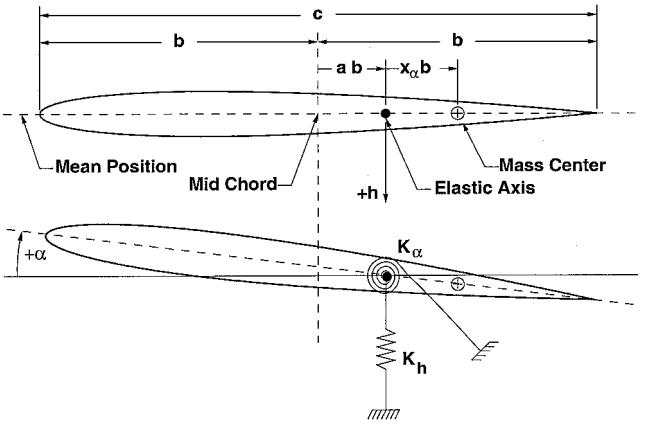

Fig. 12 Geometry for typical (pitch/plunge) two-degree-of-freedom airfoil section aeroelastic model.

and for a specified $\boldsymbol{M}$, $\boldsymbol{K}$, V, and μ, Eq. (32) then defines an eigenvalue problem with complex valued eigenvalue $\bar{\omega}^2$ and corresponding eigenvector $\boldsymbol{u}$.

Given an aeroelastic configuration where a neutral stability condition exists, for some reduced velocity V_f, the eigenvalue, that is, reduced frequency $\bar{\omega}_f$, will be purely real valued, and the aeroelastic system will have a corresponding structural eigenvector that satisfies

$$\left[-\bar{\omega}_f^2 \boldsymbol{M} + \left(1/V_f^2\right)\boldsymbol{K}\right]\boldsymbol{u}_f = (4/\pi\mu)\boldsymbol{E}(\bar{\omega}_f)\boldsymbol{u}_f \tag{33}$$

where

$$\boldsymbol{u}_f = \begin{Bmatrix} \bar{h}_f/b \\ \bar{\alpha}_f \end{Bmatrix} = \bar{\alpha}_f \begin{Bmatrix} (\bar{h}/\bar{\alpha}b)_f \\ 1 \end{Bmatrix} \tag{34}$$

Nonlinear Aerodynamics

Considering now finite amplitude, yet still harmonically varying, excitations, the right-hand side of Eq. (27) is then a nonlinear function of the structural displacement vector $[\boldsymbol{f} = \boldsymbol{f}(\boldsymbol{u}, \bar{\omega})]$. To proceed with the nonlinear multiple-degree-of-freedom LCO analysis, we begin by rewriting Eq. (27) as

$$[-\bar{\omega}^2 \boldsymbol{M} + (1/V^2)\boldsymbol{K}]\boldsymbol{v} = (4/\pi\mu\bar{\alpha})\boldsymbol{f}(\bar{\alpha}, \boldsymbol{v}, \bar{\omega}) \tag{35}$$

where

$$\boldsymbol{v} = \begin{Bmatrix} \bar{h}/\bar{\alpha}b \\ 1 \end{Bmatrix} \tag{36}$$

Next, we consider a prescribed unsteady LCO pitch amplitude $\bar{\alpha}_{\text{LCO}}$ and a purely real-valued reduced frequency. At the LCO condition, Eq. (35) can then be written as

$$\left[-\bar{\omega}_{\text{LCO}}^2 \boldsymbol{M} + \left(1/V_{\text{LCO}}^2\right)\boldsymbol{K}\right]\boldsymbol{v}_{\text{LCO}} = (4/\pi\mu\bar{\alpha}_{\text{LCO}})\boldsymbol{f}(\bar{\alpha}_{\text{LCO}}, \boldsymbol{v}_{\text{LCO}}, \bar{\omega}_{\text{LCO}}) \tag{37}$$

In this form, Eq. (37) represents a system of four equations (considering the real and imaginary parts) for the four unknowns of $\bar{\omega}_{\text{LCO}}$, V_{LCO}, $\text{Re}(\bar{h}/\bar{\alpha}b)_{\text{LCO}}$, and $\text{Im}(\bar{h}/\bar{\alpha}b)_{\text{LCO}}$.

LCO Solution Procedure

Defining $\boldsymbol{R}(\boldsymbol{L})$ as the vector operator representing the residual of the real and imaginary parts of Eq. (37), one may express $\boldsymbol{R}(\boldsymbol{L})$ as (the LCO subscript here has been dropped)

$$\boldsymbol{R}(\boldsymbol{L}) = \boldsymbol{D}\tilde{\boldsymbol{v}} - (4/\pi\mu\bar{\alpha})\tilde{\boldsymbol{f}} = \boldsymbol{0} \tag{38}$$

where $\boldsymbol{D}$ is the 4×4 matrix

$$\boldsymbol{D} = -\bar{\omega}^2 \begin{bmatrix} \boldsymbol{M} & \boldsymbol{0} \\ \boldsymbol{0} & \boldsymbol{M} \end{bmatrix} + \frac{1}{V^2} \begin{bmatrix} \boldsymbol{K} & \boldsymbol{0} \\ \boldsymbol{0} & \boldsymbol{K} \end{bmatrix} \tag{39}$$

$\tilde{\boldsymbol{v}}$ and $\tilde{\boldsymbol{f}}$ are

$$\tilde{\boldsymbol{v}} = \begin{Bmatrix} \mathrm{Re}(\bar{h}/\bar{\alpha}b) \\ 1 \\ \mathrm{Im}(\bar{h}/\bar{\alpha}b) \\ 1 \end{Bmatrix} \tag{40}$$

$$\tilde{\boldsymbol{f}} = \begin{Bmatrix} -\mathrm{Re}[\bar{c}_l(\bar{\alpha}, \bar{\omega}, \bar{h}/\bar{\alpha}b)] \\ 2\,\mathrm{Re}[\bar{c}_m(\bar{\alpha}, \bar{\omega}, \bar{h}/\bar{\alpha}b)] \\ -\mathrm{Im}[\bar{c}_l(\bar{\alpha}, \bar{\omega}, \bar{h}/\bar{\alpha}b)] \\ 2\,\mathrm{Im}[\bar{c}_m(\bar{\alpha}, \bar{\omega}, \bar{h}/\bar{\alpha}b)] \end{Bmatrix} \tag{41}$$

and $\boldsymbol{L}$ is the vector of unknown LCO variables

$$\boldsymbol{L} = \begin{Bmatrix} V \\ \bar{\omega} \\ \mathrm{Re}(\bar{h}/\bar{\alpha}b) \\ \mathrm{Im}(\bar{h}/\bar{\alpha}b) \end{Bmatrix} \tag{42}$$

We have found that a Newton–Raphson technique appears to be an efficient and stable method for quickly solving Eq. (38). That is, for a specified pitch amplitude $\bar{\alpha}$, one can implement an iterative process whereby the $(n+1)$th update to the LCO solution is given by

$$\boldsymbol{L}^{n+1} = \boldsymbol{L}^n - \left[\frac{\partial \boldsymbol{R}(\boldsymbol{L}^n)}{\partial \boldsymbol{L}}\right]^{-1} \boldsymbol{R}(\boldsymbol{L}^n) \tag{43}$$

We have found that one may use simple forward finite differencing to compute the column vectors of $\partial \boldsymbol{R}(\boldsymbol{L}^n)/\partial \boldsymbol{L}$. That is,

$$\left[\frac{\partial \boldsymbol{R}(\boldsymbol{L})}{\partial \boldsymbol{L}}\right] = \left[\begin{array}{cccc} | & | & | & | \\ \dfrac{\partial \boldsymbol{R}}{\partial V} & \dfrac{\partial \boldsymbol{R}}{\partial \bar{\omega}} & \dfrac{\partial \boldsymbol{R}}{\partial \mathrm{Re}(\bar{h}/\bar{\alpha}b)} & \dfrac{\partial \boldsymbol{R}}{\partial \mathrm{Im}(\bar{h}/\bar{\alpha}b)} \\ | & | & | & | \end{array}\right] \tag{44}$$

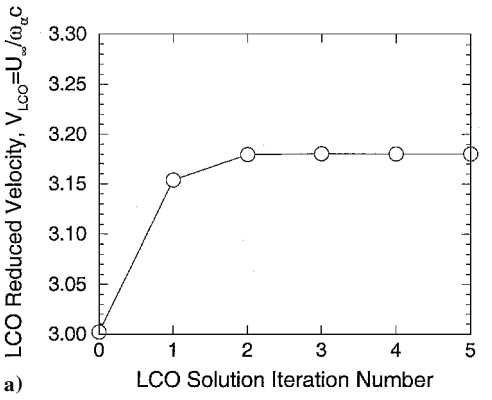

a)

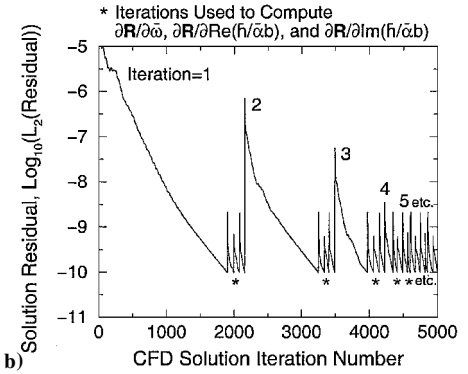

b)

Fig. 13 LCO iterative solution procedure: NACA 64A010A airfoil section, $M_\infty = 0.8$, $\alpha_0 = 0.0$ deg, and $a = -0.6$, and $\bar{\alpha} = 2.0$ deg: a) LCO reduced velocity convergence history as a function of iteration in LCO solution technique and b) harmonic balance unsteady solution convergence history as a function of iteration in LCO solution technique.

where, for example,

$$\frac{\partial \boldsymbol{R}(\boldsymbol{L}^n)}{\partial V} \approx \frac{\boldsymbol{R}(\boldsymbol{L}^n, V^n + \epsilon) - \boldsymbol{R}(\boldsymbol{L}^n, V^n)}{\epsilon} \tag{45}$$

$$\frac{\partial \boldsymbol{R}(\boldsymbol{L}^n)}{\partial \bar{\omega}} \approx \frac{\boldsymbol{R}(\boldsymbol{L}^n, \bar{\omega}^n + \epsilon) - \boldsymbol{R}(\boldsymbol{L}^n, \bar{\omega}^n)}{\epsilon} \tag{46}$$

etc., for a small ϵ.

For each step of the LCO solution procedure, the harmonic balance flow solver is implemented using the current LCO frequency $\bar{\omega}$ and structural mode shape $\bar{h}/\bar{\alpha}b$ for the prescribed LCO pitch amplitude $\bar{\alpha}$ to provide an update for the LCO unsteady aerodynamic coefficients $\bar{c}_l$ and $\bar{c}_m$. The technique is marched until a suitable level of convergence is achieved. The linear flutter solution by the use of a time-linearized aerodynamic analysis has been found to provide

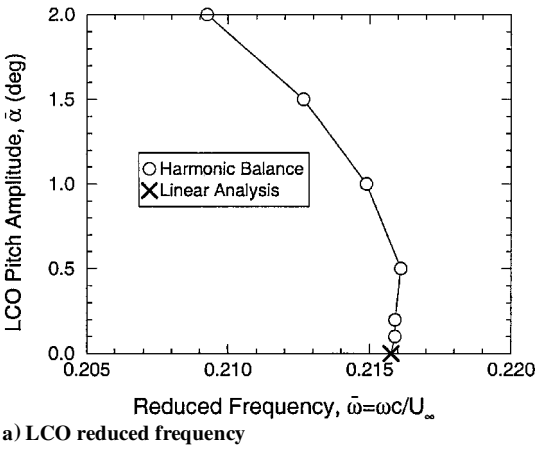

a) LCO reduced frequency

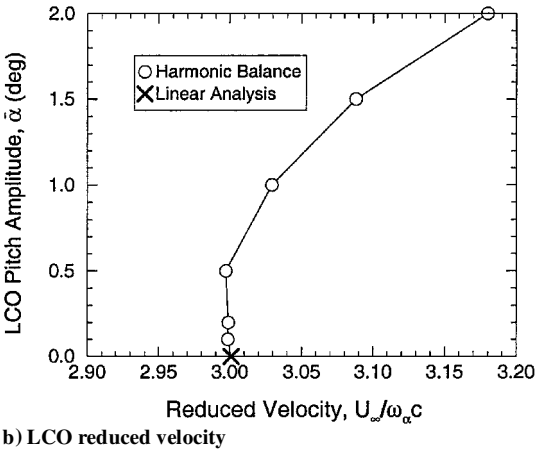

b) LCO reduced velocity

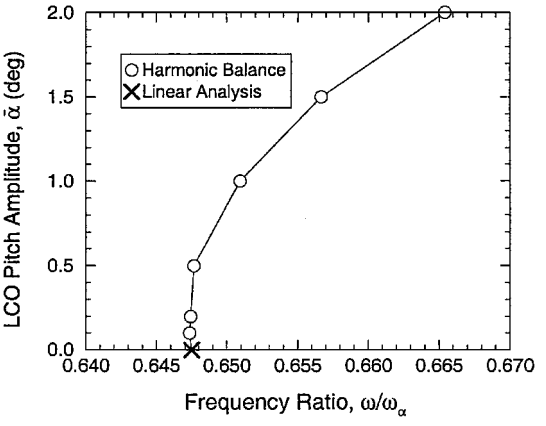

c) LCO frequency ratio

Fig. 14 Effect of pitch amplitude on LCO reduced velocity, LCO reduced frequency, and LCO frequency ratio for two-degree-of-freedom structural model: NACA 64A010A airfoil section, $M_\infty = 0.8$, $\alpha_0 = 0.0$ deg, and $a = -0.6$.

an excellent starting solution for the iterative process, and typically only a few iterations are required to achieve convergence, as will be shown in the following section.

Sample Two-Degree-of-Freedom Configuration

To demonstrate the LCO solution technique, we consider the same transonic airfoil configuration studied in the preceding sections with the following structural parameters:

$$x_\alpha = 0.25, \qquad r_\alpha^2 = 0.75, \qquad \omega_h/\omega_\alpha = 0.5, \qquad \mu = 75$$

By the use of a time-linearized flutter analysis, the flutter reduced frequency, reduced velocity, and frequency ratio can be shown to be

$$\bar{\omega}_f = 0.2158, \qquad V_f = 3.001, \qquad \omega_f/\omega_\alpha = 0.6475$$

and the corresponding flutter mode shape is

$$\boldsymbol{v}_f = \begin{Bmatrix} (7.151, 1.951) \\ 1 \end{Bmatrix} = \begin{Bmatrix} (0.1248, 0.03405)\text{per deg} \\ 1 \end{Bmatrix}$$

As can be seen, the structural mode shape at neutral stability is primarily dominated by plunging motion.

For the following LCO results, pitch amplitudes of $\bar{\alpha} = 0.1$, 0.2, 0.5, 1.0, 1.5, and 2.0 deg are considered. To illustrate the LCO iterative solution procedure described in the preceding section, Fig. 13a shows the computed LCO reduced velocity after the first five iterations of the LCO solution process for the case of the maximum pitch amplitude $\bar{\alpha} = 2.0$ deg. The zeroth iteration corresponds to the linear flutter solution of $V = 3.001$. As can be seen, only a few iterations are required to converge the solution to the LCO reduced velocity of $V = 3.1801$.

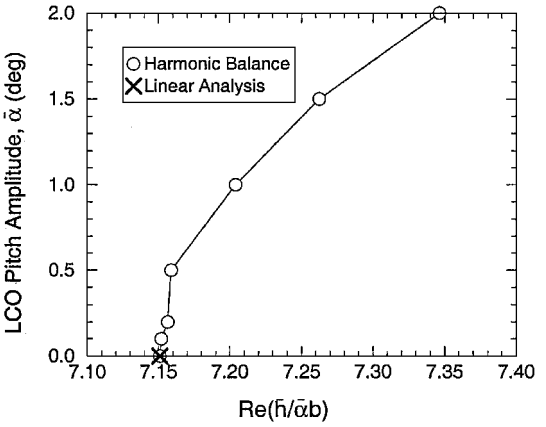

a) Real part of LCO structural mode shape

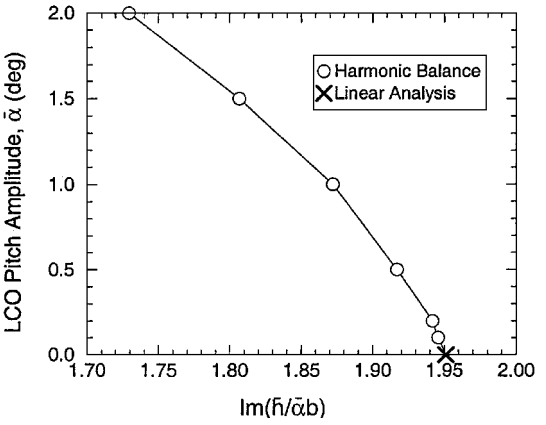

b) Imaginary part of LCO structural mode shape

Fig. 15 Effect of pitch amplitude on LCO structural mode shape for two-degree-of-freedom structural model: NACA 64A010A airfoil section, $M_\infty = 0.8$, $\alpha_0 = 0.0$ deg, and $a = -0.6$.

Figure 13b shows the corresponding convergence history of the harmonic balance solver in determining the unsteady aerodynamic lift and moment during the iterative process. The interations used to compute the columns of $\partial \boldsymbol{R}(\boldsymbol{L}^n)/\partial \boldsymbol{L}$ are also indicated. In this instance, we have approximated the gradients using

$$\frac{\partial \boldsymbol{R}(\boldsymbol{L}^n)}{\partial V} \approx \frac{\boldsymbol{R}[\boldsymbol{L}^n, V^n(1+\epsilon)] - \boldsymbol{R}(\boldsymbol{L}^n, V^n)}{\epsilon V^n} \tag{47}$$

$$\frac{\partial \boldsymbol{R}(\boldsymbol{L}^n)}{\partial \bar{\omega}} \approx \frac{\boldsymbol{R}[\boldsymbol{L}^n, \bar{\omega}^n(1+\epsilon)] - \boldsymbol{R}(\boldsymbol{L}^n, \bar{\omega}^n)}{\epsilon \bar{\omega}^n} \tag{48}$$

etc., with an $\epsilon = 0.001$ (i.e., a 10th of a percent variation of each LCO variable), which is valid in this case because each of the LCO solution variables is nonzero. Iterations for the gradient $\partial \boldsymbol{R}/\partial V$ are unnecessary and not applicable because the harmonic balance flow solver is not a function of the reduced velocity V. As can be seen, as the iterative procedure approaches the converged LCO solution, fewer and fewer iterations are required of the harmonic balance solver.

Next, Fig. 14 shows the computed LCO reduced frequency (Fig. 14a), reduced velocity (Fig. 14b), and frequency ratio (Fig. 14c) as a function of the LCO pitch amplitude. For small amplitudes, the LCO solution approaches the linear flutter solution as is expected. Note that the result for the LCO pitch amplitude vs reduced velocity curve (Fig. 14b) bends to the right, which is indicative of a stable LCO.

Finally, Fig. 15 shows the results for the real, or in-phase (Fig. 15a), and imaginary, or out-of-phase (Fig. 15b), parts of the LCO structural mode shape. Again, the solution can be seen to be rapidly converging, and, for small pitch amplitudes, the LCO solution approaches the linear flutter solution.

Conclusions

Nonlinear aerodynamic effects on divergence, flutter, and LCO for a transonic airfoil configuration are studied using a large-scale inviscid (Euler) CFD model. A new LCO solution technique is developed to determine the LCO response, based on unsteady aerodynamics provided by a frequency-domain harmonic balance solution for the nonlinear CFD model. With this technique, both stable and unstable LCO responses have been found for the same transonic airfoil. The combination of the aerodynamic harmonic balance method and the new LCO solution technique is robust and efficient and should prove to be a useful tool for studying LCO behavior.

Acknowledgments

The authors would like to acknowledge with appreciation the support of the U.S. Air Force Office of Scientific Research and Program Director, Daniel Segalman, for this work.

References

[1] Tang, D. M., Henry, J. K., and Dowell, E. H., "Limit-Cycle Oscillations of Delta Wing Models in Low Subsonic Flow," *AIAA Journal*, Vol. 37, No. 11, 1999, pp. 1355–1362.

[2] Tang, D. M., Dowell, E. H., and Virgin, L. N., "Limit Cycle Behavior of an Airfoil with a Control Surface," *Journal of Fluids and Structures*, Vol. 12, No. 7, 1998, pp. 839–858.

[3] Ueda, T., and Dowell, E. H., "Flutter Analysis Using Nonlinear Aerodynamic Forces," *Journal of Aircraft*, Vol. 21, No. 2, 1984, pp. 101–109.

[4] Greco, P. C., Jr., Lan, C. E., and Lim, T. W., "Frequency Domain Unsteady Transonic Aerodynamics for Flutter and Limit-Cycle Oscillation Prediction," AIAA Paper 97-0835, Jan. 1997.

[5] Bland, S. R., "AGARD Two-Dimensional Aeroelastic Configurations," AR-156, AGARD, 1979.

[6] Hall, K. C., Thomas, J. P., and Clark, W. S., "Computation of Unsteady Nonlinear Flows in Cascades Using a Harmonic Balance Technique," International Symposium on Unsteady Aerodynamics, Aeroacoustics and Aeroelasticity of Turbomachines, Sept. 2000.

[7] McMullen, M., Jameson, A., and Alonso, J. J., "Acceleration of Convergence to Periodic Steady State in Turbomachinery Flows," AIAA Paper 2001-0152, Jan. 2001.

E. Livne
Associate Editor